Risedronate metal complexes potentially active against Chagas disease

Bruno Demoro[a], **Francesco Caruso**[b], **Miriam Rossi**[c], **Diego Benítez**[d], **Mercedes Gonzalez**[d], **Hugo Cerecetto**[d], **Beatriz Parajón-Costa**[e], **Jorge Castiglioni**[f], **Melina Galizzi**[g], **Roberto Docampo**[g], **Lucía Otero**[a,*], and **Dinorah Gambino**[a,*]

[a] Cátedra de Química Inorgánica, DEC, Facultad de Química, Universidad de la República, Gral. Flores 2124, C. C. 1157, 11800 Montevideo, Uruguay

[b] Istituto Chimica Biomolecolare, CNR, Ple. Aldo Moro, 5, 00185, Rome, Italy

[c] Department of Chemistry, Vassar College, Poughkeepsie, New York 12604-0484, USA

[d] Departamento de Química Orgánica, Facultad de Química-Facultad de Ciencias, Universidad de la República, Iguá 4225, Montevideo, Uruguay

[e] Centro de Química Inorgánica (CEQUINOR/CONICET-UNLP), C.C. 962, Facultad de Ciencias Exactas, Universidad Nacional de La Plata, 1900 La Plata, Argentina

[f] LAFIDESU, DETEMA, Facultad de Química, Universidad de la República, Gral. Flores 2124, C. C. 1157, 11800 Montevideo, Uruguay

[g] Center for Tropical and Emerging Global Diseases and Department of Cellular Biology, University of Georgia, Athens, USA

Abstract

In the search for new metal-based drugs for the treatment of Chagas disease, the most widespread Latin American parasitic disease, novel complexes of the bioactive ligand risedronate (Ris, (1-hydroxy-1-phosphono-2-pyridin-3-yl-ethyl)phosphonate), $[M^{II}(Ris)_2]\cdot 4H_2O$, where M Cu, Co, Mn and Ni, and $[Ni^{II}(Ris)_2(H_2O)_2]\cdot H_2O$ were synthesized and characterized by using analytical measurements, thermogravimetric analyses, cyclic voltammetry and infrared and Raman spectroscopies. Crystal structures of $[Cu^{II}(Ris)_2]\cdot 4H_2O$ and $[Ni^{II}(Ris)_2(H_2O)_2]\cdot H_2O$ were solved by single crystal X-ray diffraction methods. The complexes, as well as the free ligand, were evaluated *in vitro* against epimastigotes and intracellular amastigotes of the parasite *T. cruzi*, causative agent of Chagas disease. Results demonstrated that the coordination of risedronate to different metal ions improved the antiproliferative effect against *Trypanosoma cruzi,* exhibiting growth inhibition values against the intracellular amastigotes ranging the low micromolar levels. In addition, this strong activity could be related to high inhibition of farnesyl diphosphate synthase enzyme. On the other hand, protein interaction studies showed that all the complexes strongly interact with albumin thus providing a suitable means of transporting them to tissues *in vivo*.

Keywords

Chagas disease; *Trypanosoma cruzi*; risedronate metal complexes

*Corresponding authors fax number: +59829241906, phone: +59829249739, dgambino@fq.edu.uy, luotero@fq.edu.uy.

1. Introduction

American trypanosomiasis or Chagas disease, caused by the protist parasite *Trypanosoma cruzi* (*T. cruzi*), is a major health concern in Latin America. Despite the decrease in the incidence of new infections through enforcement of public health programs, e.g. vector control, it continues to be endemic in large areas of Central and South America. The chemotherapy of this parasitic infection remains undeveloped and no effective method of immune prophylaxis is available. The treatment has been based on old and quite unspecific nitroaromatic drugs that have significant activity only in the acute phase of the disease and cause severe side effects [1–6].

The development of bioactive metal complexes is a promising new approach in the search for a treatment of Chagas disease. In this sense, a strategy based on the synthesis of complexes combining ligands bearing antiparasitic activity and suitable metal ions has been successfully developed [7–8]. In general, these metal compounds may have dual or even multiple mechanisms of action by combining the pharmacological properties of both the ligand and the metal, leading to a synergistic or an additive effect. In addition, an improvement of ligand's bioavailability could be achieved by complex formation. This approach led us to develop a variety of bioactive metal complexes whose mechanisms of action were extensively studied [9–20].

We are currently involved in the development of metal complexes with bioactive bisphosphonates as ligands. Bisphosphonates are pyrophosphate analogues in which the oxygen bridge between the two phosphorus atoms has been replaced by a carbon substituted with various side chains (Fig. 1). According to a current pharmaceutical development practice, great efforts are being made to get new therapeutic tools for certain diseases by evaluating well established drugs, clinically used for the treatment of other pathologies [21,22]. In this sense, several bisphosphonates that are in clinical use for the treatment of bone diseases are active against *T. cruzi* [23,24]. The discovery of significant amounts of inorganic polyphosphates, stored in parasite-specific organelles called acidocalcisomes, suggested that analogues to condensed phosphates, like bisphosphonates, could inhibit the parasite growth [25]. The main target of these compounds is the parasitic farnesyl diphosphate synthase enzyme (TcFPPS) which is involved in the biosynthesis of polyisoprenoids and sterols. This enzyme is competitively inhibited by commercial bisphosphonate drugs, like risedronate ((1-hydroxy-1-phosphono-2-pyridin-3-yl-ethyl)phosphonate, Ris) (Figure 1) [26,27]. Risedronate is not only an inhibitor of *in vitro* parasite growth but it significantly reduces the parasitemia in infected mice and increases the animal survival with no toxicity [28,29]. However, a significant clinical disadvantage of bisphosphonates is their poor oral bioavailability (less than 1 %) due to the high ionization of phosphonate groups at physiological pH [30]. This disadvantage could potentially be attenuated through coordination to a metal ion.

In this work, the synthesis and characterization of five novel risedronate complexes, $[M^{II}(Ris)_2]\cdot 4H_2O$, with M = Cu, Co, Mn and Ni, and $[Ni^{II}(Ris)_2(H_2O)_2]\cdot H_2O$, are presented. Their *in vitro* antiproliferative effect on *T. cruzi* epimastigotes and amastigotes is evaluated and compared to that of the free risedronate ligand. In addition, the ability of the obtained complexes of inhibiting TcFPPS is evaluated. Moreover, their interaction with albumin is studied, since it could provide a way to transport the complexes *in vivo* in the blood.

2. Experimental

2.1 Materials

Common laboratory chemicals were purchased from commercial sources and used without further purification. Sodium salt of risedronate (NaRis, $C_7H_{10}NO_7P_2Na\cdot2.5H_2O$) was provided by Gerardo Ramón Uruguay S.A.

2.2 Syntheses of [M^{II}(Ris)$_2$]·4H$_2$O, with M = Mn, Co, Ni, Cu

2.2.1 General procedure—NaRis (50 mg, 0.14 mmol) was dissolved in 5 mL of water and the solution's pH value was adjusted to 2.0 by addition of HCl solution. The corresponding amount (0.07 mmol) of $MCl_2\cdot xH_2O$ (with M = Mn, Co, Ni and Cu and x = 4, 6, 6, 2, respectively) was added. After 24 h at room temperature, a solid was filtered off.

[Mn^{II}(Ris)$_2$]·4H$_2$O (Yield: 25 mg, 50%) was obtained as a white microcrystalline solid. Found: C, 24.3; H, 4.1; N, 4.1; H_2O, 10.4. Calc. for $C_{14}H_{28}N_2O_{18}P_4Mn$: C, 24.3; H, 4.0; N, 4.0; H_2O, 10.4 %.

[Co^{II}(Ris)$_2$]·4H$_2$O (Yield: 26 mg, 46%) was obtained as a light pink microcrystalline solid. Found: C, 24.1; H, 4.1; N, 4.1; H_2O, 10.4. Calc. for $C_{14}H_{28}N_2O_{18}P_4Co$: C, 24.2; H, 4.0; N, 4.0; H_2O, 10.6 %.

[Ni^{II}(Ris)$_2$]·4H$_2$O (Yield: 33 mg, 67%) was obtained as a greenish microcrystalline solid. Found: C, 24.1; H, 4.1; N, 4.0; H_2O, 10.4. Calc. for $C_{14}H_{28}N_2O_{18}P_4Ni$: C, 24.2; H, 4.0; N, 4.0; H_2O, 10.5 %.

[Cu^{II}(Ris)$_2$]·4H$_2$O (Yield: 17 mg, 34%) was obtained as sky blue prismatic crystals. Found: C, 24.1; H, 4.1; N, 4.0; H_2O, 10.3. Calc. for $C_{14}H_{28}N_2O_{18}P_4Cu$: C, 24.0; H, 4.0; N, 4.0; H_2O, 10.1 %.

2.2.2 Synthesis of [Ni^{II}(Ris)$_2$(H$_2$O)$_2$]·2H$_2$O—Light green crystals of [Ni^{II}(Ris)$_2$(H$_2$O)$_2$] ·2H$_2$O were obtained along with [Ni^{II}(Ris)$_2$]·4H$_2$O complex from the same synthetic procedure.

[Ni^{II}(Ris)$_2$(H$_2$O)$_2$]·2H$_2$O (Yield: 31 mg, 25 %). Found: C, 24.35; H, 4.0; N, 4.1. Calc. for $C_{14}H_{28}N_2O_{18}P_4Ni$: C, 24.2; H, 4.0; N, 4.0 %.

2.3 Physicochemical characterization

C, H and N analyses were performed with a Carlo Erba Model EA1108 elemental analyzer. Thermogravimetric measurements (TGA) were done on a Shimadzu TGA 50 thermobalance, with a platinum cell, working under flowing nitrogen (50 mL min^{-1}) and at a heating rate of 0.5 °C min^{-1} (RT - 80 °C range) and 1.0 °C min^{-1} (80 °C – 350 °C range). FTIR spectra (4000– 200 cm^{-1}) of the complex and the free ligand were measured as KBr or CsI pellets with a Bomen FTIR model M102 instrument. Raman spectra were scanned with the FRA 106 accessory of a Bruker IF 66 FTIR spectrophotometer. The 1064 nm radiation of a Nd:YAG laser was used for excitation and 50–60 scans were routinely accumulated.

2.4 Crystallographic study

Suitable crystals for X-ray diffraction data were obtained from the synthesis solution. Data of the copper and nickel complexes were collected at 125(2) K by using graphite monochromated Mo Ka radiation (λ = 0.710 73 Å) in a Bruker SMART APEX II CCD X-ray diffractometer. Structure resolution and refinement were performed using ShelX [31]. Details are included in Table 1. Those H atoms not found in Fourier maps were included from models and constrained

as riding on their bound atoms. These crystal structures have been deposited as CCDC 733164 & 733165.

2.5 Cyclic Voltammetry studies

Electrochemical behavior was studied by cyclic voltammetry. Cyclic voltammograms were obtained with a Epsilon Electrochemical Analyzer. A standard electrochemical three electrode cell of volume 10 mL completed the system. Hanging drop mercury electrode (HDME) was employed as working electrode. A platinum wire was used as counter electrode, while a Ag/AgCl electrode was used as a reference electrode. Measurements were performed at room temperature in 0.5 mM aqueous solutions of the complexes (phosphate buffer 0.1 M, pH=7). The corresponding 0.1 M buffer solution was used as supporting electrolyte. Solutions were deoxygenated *via* purging with nitrogen for 15 minutes prior to the measurements. A continuous gas stream was passed over the solution during the measurements.

2.6 *In vitro* activity on *T. cruzi* epimastigotes

Handling of live *T. cruzi* was done according to established guidelines [32]. The epimastigote form of the parasite Tulahuen 2 strain was grown at 28 °C in an axenic medium (Brain-Heart Infusion (BHI)-Tryptose Agar), complemented with 5 % fetal calf serum. Cells from a 5 days-old culture were inoculated into 50 mL of fresh culture medium to give an initial concentration of 1×10^6 cells/mL. Cell growth was followed by daily measuring the absorbance A of the culture at 600 nm for 5 days. Before inoculation, the media was supplemented with a 25 μM dose of the risedronate metal compounds by addition of an appropiate aliquot of a stock buffer phosphate solution pH 7.2, 5.5 M in glucose. The compounds ability to inhibit the growth of the parasite was evaluated, in triplicate, in comparison to the control (no drug added to the media). The control was run in the absence of any drug. Metal salts showed no effect on parasite growth. The percentage of growth inhibition (PGI) was calculated as follows: % = {1−[(Ap −A_0p)/(Ac−A_0c)]}×100, where Ap=A_{600} of the culture containing the drug at day 5; A_0p=A_{600} of the culture containing the drug just after addition of the inocula (day 0); Ac=A_{600} of the culture in the absence of any drug (control) at day 5; A_0c=A_{600} in the absence of the drug at day 0 [12]. Reported values are mean of three independent experiments with a SD less than 10%.

2.7 Drug screening assays in Vero cells and *T. cruzi* intracellular amastigotes

Gamma-irradiated (2,000 Rads) Vero cells (3.4×10^4 cells/well) were seeded in 96 well plates (black, clear bottom plates from Greiner Bio-One) in 100 μL RPMI media (Sigma) with 10 % FBS. Plates were incubated overnight at 35 °C and 7 % CO_2. After overnight incubation, Vero cells were challenged with 3.4×10^5 trypomastigotes/well (CL strain overexpressing a tdTomato red fluorescent protein [33]) in 50 μL volume and incubated for 5 h at 35 °C and 7 % CO_2. After infection, wells were washed once with Hanks solution (150 μL/well) to eliminate any extracellular parasites and compounds were added in serial dilutions in RPMI media in 150 μL volumes. Each dilution was tested in quadruplicate. Each plate also contained controls with host cells and no parasites (for background check), controls with two representative drug dilutions and no parasites (for cytotoxicity assays), and controls with parasites and no drugs (positive control). For each plate, benznidazole was also used as a positive control at 3.5 and 1.5 μM. After drug addition, plates were incubated at 35 °C and 7 % CO_2. At day 3 post-infection, plates were assayed for fluorescence. IC_{50} values were determined by non-linear regression analysis using SigmaPlot.

2.8 TcFPPS inhibition assay

One hundred microliters of assay buffer (10 mM Hepes (4-(2-hydroxyethyl)-1-piperazineethanesulfonic acid), pH 7.4, 5 mM $MgCl_2$, 2 mM dithiothreitol, 100 μM [4-^{14}C]

IPP (isopentenyl diphosphate) (10 μCi/μmol)) and 100 μM DMAPP (dimethylallyl pyrophosphate) were prewarmed to 37 °C. The assay was initiated by the addition of recombinant protein (10–20 ng). The assay was allowed to proceed for 30 min at 37 °C and was quenched by the addition of 6 M HCl (10 μL). The reaction mixtures were made alkaline with 6.0 M NaOH (15 μL), diluted in water (0.7 mL), and extracted with hexane (1 mL). The hexane solution was washed with water and transferred to a scintillation vial for counting. One unit of enzyme activity was defined as the activity required to incorporate 1 nmol of [4-^{14}C] IPP into [14-^{14}C]FPP (farnesyl diphosphate) in 1 min. IC_{50} values were determined by non-linear regression analysis using SigmaPlot.

2.9 Interaction with proteins

The interaction of the complexes with albumin (BSA) was performed according to previously reported methods [34]. BSA (500 μM) and metal complexes in a 1:1 molar relationship were incubated at 37 °C in 100 mM phosphate buffer, pH 7.4, 0.15 M NaCl, for 48 h. BSA (including BSA with bound metal complex) was separated from the other components of the solution (unbound metal complex) based in their significantly different molecular weights. For this purpose the incubated solutions were ultrafiltrated using Centrikon tubes (10000 Da cut-off). The amount of unbound complex in the filtrate was quantified by atomic absorption spectrometry using a Perkin Elmer 5000 spectrometer.

3. Results and Discussion

3.1 Chemistry

Five new metal complexes using risedronate (Figure 1) as ligand have been synthesized and fully characterized. Unlike earlier studies in which high temperature and pressure conditions were used in the synthesis of bisphophonate metal complexes, [35] we obtained good yields and high purities of $[M^{II}(Ris)_2]\cdot 4H_2O$, with M = Cu, Mn, Co, Ni, and $[Ni^{II}(Ris)_2(H_2O)_2]\cdot 2H_2O$ by direct synthesis in aqueous solution at room temperature. Analytical data, including thermogravimetric analysis results confirmed the proposed formula.

3.2 Thermal analysis

All the obtained $[M^{II}(Ris)_2]\cdot 4H_2O$ complexes showed a single weight loss, corresponding to the four water molecules of crystallization. This agrees with the single peak observed in the infrared spectra of the complexes (see below) that corresponds to a population of similarly bound lattice water molecules. $[Cu^{II}(Ris)_2]\cdot 4H_2O$ showed a 10.1% weight loss at 131.3 °C. A sharp peak was observed in DTG (derivative thermogravimetry). However, for the rest of the metal complexes, the corresponding weight loss was observed as a broad step in the 80–140 °C range. This difference can be related either to a different degree of complex crystallinity or to the presence of different types of hydrates: a lattice stoichiometric hydrate for the first and a channel-type hydrate for the others [36].

Another weight loss near 260 °C for all the complexes was observed and could correspond to complex decomposition.

3.3 Infrared and Raman studies

Significant infrared vibration bands, useful for determining the ligand mode of coordination, were tentatively assigned for the complexes and are shown in Table S1 (Supplementary information). Raman spectra analysis allowed performing a better assignment of the infrared bands. The ligand and all the complexes showed typical bands of bisphosphonic acid derivatives in the 900–1300 cm^{-1} region; these overlapped with some of the pyridinic ring deformation bands, making it difficult to assign the corresponding bands, both in Raman and

infrared spectra. Moreover, in this region, modifications of band wave numbers after complex formation could not be unequivocally attributed to coordination because, as previously described for different risedronate hydrates, hydrogen bond formation itself would affect the vibrational spectrum [36]. It should be noted that infrared and Raman spectra of the $[M^{II}(Ris)_2]\cdot4H_2O$ complexes are almost identical in this region but different from the $[Ni^{II}(Ris)_2(H_2O)_2]\cdot2H_2O$ complex suggesting similar structures for the former.

In the 1100–1250 cm^{-1} region, POO$^-$ symmetric and asymmetric stretching bands are observed. These are shifted to lower wave numbers when compared to the free risedronate ligand, at 1134 and 1210 cm^{-1}. This fact, along with the shift of P-OH stretching band at 2150 cm^{-1} to lower wave numbers, is consistent with the coordination of risedronate ligand through the phosphonate groups in all the obtained metal complexes [37,38].

In the 3350 cm^{-1} region, a broad band can be assigned to OH bond stretching of the C-OH group, since this group forms hydrogen bonds both in the free ligand and in the complexes [36]. This band slightly shifts as a consequence of coordination and/or hydrogen bonds in $[M^{II}(Ris)_2]\cdot4H_2O$ complexes, while for $[Ni^{II}(Ris)_2(H_2O)_2]\cdot2H_2O$ it shifts to lower wave numbers (3242 cm^{-1}) in accordance to the different involvement of this group in the different complexes. In addition, a higher shift in the wave number of the C-P stretching band (at 1385 cm^{-1} for the free ligand) is observed for $[M^{II}(Ris)_2]\cdot4H_2O$ complexes compared to $[Ni^{II}(Ris)_2(H_2O)_2]\cdot2H_2O$, agreeing with a tridentate and bidentate coordination, respectively.

No changes were observed in bands assigned to the 3-substituted pyridine ring as it does not participate in the coordination to the metals [39,40]. However, in the Raman spectra, two intense bands at 1023 and 1055 cm^{-1} corresponding to the in-plane pyridine ring deformation of the risedronate ligand, appear as a single band in the 1050–1060 cm^{-1} region for all $[M^{II}(Ris)_2]\cdot4H_2O$ complexes. This would imply participation of the pyridine nitrogen in intermolecular out of plane hydrogen bonds in the complexes, as previously reported for the different hydrates of the ligand [36].

The presence of a unique population of constrained water molecules in the crystal lattice of all complexes was evident since a sharp peak at c.a. 3500 cm^{-1}, corresponding to water OH stretching, was observed [36]. Additionally, a broad band centered at 3300 cm^{-1} characteristic of hydrogen bonded OH functionality was observed for all obtained complexes. For $[Ni^{II}(Ris)_2(H_2O)_2]\cdot2H_2O$ complex, weak bands at 825, 575 and 485 cm^{-1} could be related to coordinated water molecules [37].

3.4 Crystal structure of $[Cu^{II}(Ris)_2]\cdot4H_2O$

Crystals of $[Cu^{II}(Ris)_2]\cdot4H_2O$, suitable for X-ray diffraction methods, came out of synthesis solution after 24 h standing at room temperature. Relevant intra-molecular bond distances and angles around the metal ion are shown in Table 2. Fig. 2 depicts a drawing of the molecule including labels of main non-H atoms and displacement ellipsoids at the 50% probability level.

The X-ray diffraction study showed that the complex $[Cu^{II}(Ris)_2]$ consists of discrete monomeric molecules. Both risedronate ligands coordinate the copper atom in a tridentate manner through two oxygen atoms, one from each phosphonate group, and another oxygen belonging to the C-OH moiety. Both coordinating phosphonate oxygen atoms are deprotonated while the C-OH group remains protonated. Additionally, the pyridine nitrogen is protonated resulting in a −1 net charge for each ligand. Both ligands are equivalent; the metal atom resides on an inversion center.

The geometry around copper atom, according to the obtained bond distances and angles, could be described as intermediate between octahedral and square-planar. Equatorial oxygen atoms

(O3, O3a, O5 and O5a) are coplanar with the metal atom while O7 is deviated 12° from the octahedral axis. O7 position is restricted by the ligand tridentate coordination. Moreover, in agreement with the Jahn-Teller effect characteristic of ions with a d^9 electronic configuration, both axial Cu-O7 distances are longer than the equatorial ones. A related phosphonato trinuclear copper compound, catena-(piperazinium bis(μ_3-1-hydroxyethylidenediphosphonato)-tetraaqua-tri-copper) shows a more regular octahedron as seen by a shorter Jahn-Teller elongation (Cu-O = 2.46 Å) when compared with the title compound (2.655(1) Å), and less angular distortion as the widest O-Cu-O angle are 97.7° and 101.80(5)°, respectively [41]. A complex net of intermolecular hydrogen bonds stabilizes the crystal structure (Table S2). Two different populations of lattice water molecules are involved in different intermolecular hydrogen bonds i.e. O1w and O2w (Table 1S). Additionally, O4… O6 and O7…O2 bonds complete the net. The effect of the involvement of C-OH group (O7… O2) and N-H moiety (O1w…N′) on these hydrogen bonds also resulted evident through the analysis of the IR and Raman spectra.

3.5 Crystal structure of [Ni^{II}(Ris)$_2$(H$_2$O)$_2$]·2H$_2$O

Single crystals of [Ni^{II}(Ris)$_2$(H$_2$O)$_2$]·2H$_2$O, suitable for X-ray diffraction methods, were obtained from the synthesis solution after 48 h standing at room temperature. Relevant bond distances and angles around the metal ion are shown in Table 2. Fig. 3 depicts the molecular structure including selected labels and displacement ellipsoids at 50% probability level.

The X-ray diffraction study shows that the complex [Ni^{II}(Ris)$_2$(H$_2$O)$_2$]· consists of discrete monomeric molecules. Both risedronate ligands coordinate the nickel atom in a bidentate manner through two oxygen atoms, one from each phosphonate group. Two oxygen atoms from water molecules complete the coordination sphere in *trans* positions. The risedronate C-OH hydroxyl is not involved in bonding to the metal, in contrast to the Cu complex described above. Both coordinating phosphonate oxygen atoms are deprotonated while the pyridine nitrogen remains protonated resulting in a −1 net charge for each risedronate ligand. As observed for the Cu complex both ligands are equivalent, with the nickel atom residing on an inversion center. Bond distances and angles around the nickel atom are in agreement with a regular octahedral geometry. The structure shows a disordered P1 atom, see the alternative phosphorus atom (P11) in Fig. 3. A complex 3D network of hydrogen bonds stabilizes the compound in the crystal.

Coordinated water molecules and crystallization ones are involved in intramolecular hydrogen bonds (Table S2). Lattice water molecules are also involved in intermolecular hydrogen bonds. Hydrogen N…O4′ bonds complete the net. As previously stated, the effect of these hydrogen bonds on the IR and Raman spectra was evident.

There are only two risedronate complexes in the CSD database, catena-((μ_3-(1-hydroxy-1-(hydroxyphosphinato)-2-pyridin-3-ylethyl)phosphonato)-aqua-cobalt), where the risedronate anion displays charge -2, and catena-((μ_2-dihydrogen 1-hydroxy-2-(3-pyridinio) ethylidene-1,1-diphosphonate)-(μ_2-hydrogen 1-hydroxy-2-(3-pyridinio)ethylidene-1,1-diphosphonate)-gadolinium dihydrate) [42,43]. The Co and Gd complexes differ markedly from the Cu and Ni complexes reported here, because the risedronate ligand points to two different metal centers and so it stabilizes polynuclear species whereas the title compounds show chelation only on one metal center defining mononuclear arrangements.

3.6 Cyclic voltammetry studies

The complexes and the ligands were characterized by cyclic voltammetry at a hanging drop mercury electrode (HDME) in phosphate buffer, pH=7. In the present experimental conditions the different metal risedronate complexes (M-Ris) show similar behavior. They exhibit on the

forward cathodic scan one reduction process, which can be attributed to the reduction of the metal center. No signals are observed for the free ligand in the same potential range.

In order to determine if the complexes completely dissociate in aqueous solution to give metal ion and the free ligand a new set of experiments were performed. Cyclic voltammograms (CV) of the corresponding aqueous salt solutions were measured at the same experimental conditions. The results show that the electrochemical behavior and the reduction potentials of the M-Ris complexes are different from those obtained for the metal salts. Comparative voltammograms, at v = 0.1V/s, of the Cu-Ris complex and the copper salt are presented in Fig. 4, as an example. Obtained potential values for the reduction peak of M-Ris complexes and the metal salts are shown in Table 3. From the measurements, it is possible to infer that at the assayed experimental conditions, no detectable "free copper" exists in the solution of the complexes. Consequently, the main electroactive species are metal-risedronate species present in each complex solution. This fact is biologically relevant since it can be assumed that a risedronate metal compound would be the active species in the anti *T. cruzi* tests. In addition, no changes in the electrochemical signal were observed under the assayed conditions for at least the five days needed for biological studies, showing that the metal risedronate species present in solution resulted stable for this time period.

3.7 *In vitro* anti *T. cruzi* activity

The complexes *in vitro* biological activities against epimastigotes of *T. cruzi* were evaluated as a screening preliminary assay. At 25 μM obtained complexes resulted toxic to the epimastigote form of the parasite being, most of them, more active than the free Ris ligand. For this reason, all complexes were tested for their activity against the intracellular amastigote form of the parasite. Results are depicted in Table 4. Additionally, the effect of the assayed complexes on the mammalian Vero cell in the absence of parasitic infection was evaluated.

Antiparasitic activity resulted evident on the intracellular amastigote form of *T. cruzi* for most of the assayed complexes. They proved to be potent inhibitors of the amastigote growth with IC_{50} values in the low micromolar range. Mn complex resulted the most active one with an IC_{50} of 14 μM. With exception of the Co complex, which was less active, all other complexes (Cu, Ni, Mn) improved the toxicity of risedronate against the amastigotes.

Additionally, citotoxicity against mammalian Vero cells was only observed in doses higher than 50 μM, which demonstrates good selectivity indexes for the most active Cu and Mn complexes.

3.8 TcFPPS inhibition assay

IC_{50} values for TcFPPS inhibition are shown in Table 4. Most of the obtained compounds were potent inhibitors of TcFPPS and the inhibition resulted stronger than that of the free Ris ligand. The efficacy of metal-Ris complexes as TcFPPS inhibitors showed a correlation with their growth inhibitory effect on amastigotes of *T. cruzi*. The most active complex in inhibiting amastigote growth (Mn), also presented the lowest IC_{50} value for TcFPPS inhibition.

3.9 Interaction with proteins

The study of metal complex interaction with proteins is particularly relevant for the development of metal-based drugs as these biomolecules present a variety of coordinating options for metal complexes. Interaction of a drug with plasma proteins could play a significant role in determining its bioavailability. For instance, plasma proteins might transport them to the corresponding target and several examples are reported in the literature, including drugs being currently evaluated in clinical trials [44–45].

Interaction of the obtained metal complexes with bovine serum albumin (BSA), as model plasma protein, was studied and results are presented in Table 5.

Results show very high levels of BSA binding in the assayed conditions. This fact could favor complexes biological activity *in vivo* by overcoming their low solubility in aqueous solution (at pH = 7, a 0.5 mM maximum concentration could be reached). Further studies will be performed to assess the actual role of proteins in the biological behavior of the complexes and will be published elsewhere.

4. Conclusions

Five novel complexes of the bioactive drug risedronate were obtained through a simple synthetic route and were completely characterized. Results demonstrated that the coordination of risedronate to different metal ions improved its antiproliferative effect against *T. cruzi* exhibiting IC_{50} values against the intracellular amastigote form of the parasite ranging the low micromolar levels. In addition, this high activity could be correlated to high inhibition of farnesyl diphosphate synthase enzyme.

On the other hand, since one of the drawbacks of using risedronate as a drug is the high ionization of phosphonate groups at physiological pH which causes its rapid elimination, metal coordination of risedronate could attenuate this biological disadvantage. Additionally, interaction with serum proteins could eventually favor risedronate metal complexes bioavailability.

In agreement with our previous research, the results of this work show that the approach of coordinating anti-trypanosomal organic compounds with metals ions can be a suitable strategy to develop novel therapeutic tools against American Trypanosomiasis.

Supplementary Material

Refer to Web version on PubMed Central for supplementary material.

Acknowledgments

References

1. Urbina JA, Docampo R. Trends Parasitol 2003;19:495–501. [PubMed: 14580960]

2. Paulino M, Iribarne F, Dubin M, Aguilera-Morales S, Tapia O, Stoppani AOM. Mini-Rev Med Chem 2005;5:499–519. [PubMed: 15892691]

3. Maya JD, Cassels B, Iturriaga-Vásquez P, Ferreira J, Faúndez M, Galanti N, Ferreira A, Morello A. Comp Biochem Physiol A 2007;146:601–620.

4. Cerecetto H, González M. Curr Topics Med Chem 2002;2:1185–1190.

5. Schofield C, Jannin J, Salvatella R. Trends Parasitol 2006;22:583–588. [PubMed: 17049308]

6. Croft S, Barret M, Urbina J. Trends Parasitol 2005;21:508–512. [PubMed: 16150644]

7. Sánchez-Delgado, RA.; Anzellotti, A.; Suárez, L. Metal ions in Biological Systems. Sigel, H.; Sigel, A., editors. Vol. 41. Marcel Dekker; New York: 2004. p. 379-419.

8. Cavalli A, Bolognesi ML. J Med Chem 2009;52:7339–7359. [PubMed: 19606868]

9. Otero L, Noblía P, Gambino D, Cerecetto H, González M, Di Maio R, Ellena J, Piro OE. Inorg Chim Acta 2003;344:85–94.

10. Cabrera E, Cerecetto H, González M, Gambino D, Noblía P, Otero L, Parajón-Costa B, Anzellotti A, Sánchez-Delgado R, Azqueta A, López de Ceráin A, Monge A. Eur J Med Chem 2004;39:377–382. [PubMed: 15072846]

11. Otero L, Aguirre G, Boiani L, González M, Denicola A, Rigol C, Olea-Azar C, Maya JD, Morello A, Gambino D, Cerecetto H. Eur J Med Chem 2006;41:1231–1239. [PubMed: 16828524]

12. Otero L, Vieites M, Boiani L, Denicola A, Rigol C, Opazo L, Olea-Azar C, Maya JD, Morello A, Luise Krauth-Siegel R, Piro OE, Castellano E, González M, Gambino D, Cerecetto H. J Med Chem 2006;49:3322–3331. [PubMed: 16722651]

13. Urquiola C, Vieites M, Aguirre G, Marín A, Solano B, Arrambide G, Lavaggi ML, Torre MH, González M, Monge A, Gambino D, Cerecetto H. Bioorg Med Chem 2006;14:5503–5509. [PubMed: 16709457]

14. Otero L, Smircich P, Vieites M, Ciganda M, Cardoso Severino P, Terenzi H, Cerecetto H, Gambino D, Garat B. J Inorg Biochem 2007;101:74–79. [PubMed: 17027974]

15. Otero L, Folch C, Barriga G, Rigol C, Opazo L, Vieites M, Gambino D, Cerecetto H, Norambuena E, Olea-Azar C. Spectrochim Acta Part A Molecular and Biomolecular Spectroscopy 2008;70:519–523.

16. Vieites M, Otero L, Santos D, Gajardo D, Toloza J, Figueroa R, Norambuena E, Olea-Azar C, Aguirre G, Cerecetto H, González M, Morello A, Maya JD, Garat B, Gambino D. J Inorg Biochem 2008;102:1033–1043. [PubMed: 18226837]

17. Vieites M, Smircich P, Parajón-Costa B, Rodríguez J, Galaz V, Olea-Azar C, Otero L, Aguirre G, Cerecetto H, González M, Gómez-Barrio A, Garat B, Gambino D. J Biol Inorg Chem 2008;13(5): 723–735. [PubMed: 18322709]

18. Vieites M, Otero L, Santos D, Olea-Azar C, Norambuena E, Aguirre G, Cerecetto H, González M, Kemmerling U, Morello A, Maya JD, Gambino D. J Inorg Biochem 2009;103:411–418. [PubMed: 19187969]

19. Benítez J, Guggeri L, Tomaz I, Arrambide G, Navarro M, Costa Pessoa J, Garat B, Gambino D. J Inorg Biochem 2009;103:609–616. [PubMed: 19091422]

20. Vieites M, Smircich P, Guggeri L, Marchán E, Gómez-Barrio A, Navarro M, Garat B, Gambino D. J Inorg Biochem 2009;103:1300–1306. [PubMed: 19361864]

21. Docampo R, Moreno SNJ. Curr Drug Targets – Infectious Disorders 2001;1:51–61.

22. Urbina J. Expert Opin Ther Patents 2003;13:661–669.

23. Widler L, Jaeggi KA, Glatt M, Müller K, Bachmann R, Bisping M, Born AR, Cortesi R, Guiglia G, Jeker H, Klein R, Ramseier U, Schmid J, Schreiber G, Seltenmeyer Y, Green JR. J Med Chem 2002;45:3721–3738. [PubMed: 12166945]

24. Sanders JM, Song YJ, Chan MW, Zhang Y, Jennings S, Kosztowski T, Odeh S, Flessner R, Schwerdtfeger C, Kotsikorou E, Meints GA, Gomez AO, Gonzalez-Pacanowska D, Raker AM, Wang H, Beek ER, Papapoulos SE, Morita CT, Oldfield E. J Med Chem 2005;48:2957–2963. [PubMed: 15828834]

25. Urbina JA, Moreno B, Vierkotter S, Oldfield E, Payares G, Sanoja C, Bailey BN, Yan W, Scott DA, Moreno SNJ, Docampo R. J Biol Chem 1999;274:33609–33615. [PubMed: 10559249]

26. Montalvetti A, Bailey BN, Martin MB, Severin GW, Oldfield E, Docampo R. J Biol Chem 2001;276 (36):33930–33937. [PubMed: 11435429]

27. Martin MB, Grimley JS, Lewis JC, Heath HT, Bailey BN, Kendrick H, Yardley V, Caldera A, Lira R, Urbina JA, Moreno SNJ, Docampo R, Croft SL, Oldfield E. J Med Chem 2001;44:909–916. [PubMed: 11300872]

28. Garzoni LR, Caldera A, Meirelles M, de Castro SL, Docampo R, Meints GA, Oldfield E, Urbina J. Int J Antimicrob Agents 2004;23:273–285. [PubMed: 15164969]

29. Garzoni RL, Waghabi MC, Baptista MM, De Castro SL, Meirelles ML, Britto CC, Docampo R, Oldfield E, Urbina JA. Int J Antimicrob Agents 2004;23:286–290. [PubMed: 15164970]

30. Vachal P, Hale JJ, Lu Z, Streckfuss EC, Mills SG, MacCoss M, Yin DH, Algayer K, Manser K, Kesisoglou F, Ghosh S, Alani LL. J Med Chem 2006;49:3060–3063. [PubMed: 16722624]

31. Sheldrick GM. Acta Crystallogr 2008;A64:112–122.

32. Huang L, Lee A, Ellman JA. J Med Chem 2002;45:676–684. [PubMed: 11806719]

33. Canavaci AM, Bustamante JM, Padilla AM, Pereza Brandan CM, Simpson LJ, Xu D, Boehlke CL, Tarleton RL. PLOS Negl Trop Dis 2010;4:e740. [PubMed: 20644616]

34. Messori L, Orioli P, Vullo D, Alessio E, Iengo E. Eur J Biochem 2000;267:1206–1213. [PubMed: 10672032]

35. Matczak-Jon E, Videnova-Adrabinska V. Coord Chem Rev 2005;249:2458–2488.

36. Redman-Furey N, Dicks M, Bigalow-Kern A, Thomas Cambron R, Lubey G, Lester C, Vaughn D. J Pharm Sci 2005;94(4):893–911. [PubMed: 15736193]

37. Nakamoto, K. Infrarred and Raman Spectra of Inorganic and Coordination compounds. 5. Wiley & Sons. Inc; New York: 1997.

38. Herlinger AW, Ferraro JR, Garcia JA, Chiarizia R. Polyhedron 1998;17:1471–1475.

39. Lin-Vien, D.; Colthup, NB.; Fataley, WWG.; Grasselli, JG. The handbook of infrared and raman characteristic frecuencies of organic molecules. 1. Academic Press; San Diego: 1991.

40. Pouchert, CJ. The Aldrich Library of FT-IR Spectra Edition. 1. Aldrich Chemical Co; United States: 1985.

41. Song HH, Zheng LM, Xin XQ. Chin J Inorg Chem 2002;18:941–944.

42. Zhang ZC, Bao SS, Zheng LM. Chin J Inorg Chem 2007;23:1851–1856.

43. Zhang ZC, Gao S, Zheng LM. Dalton Trans 2007:4681–4684. [PubMed: 17940649]

44. Dolman G, Deacon B, Hambley TW. J Inorg Biochem 2002;88:260–267. [PubMed: 11897339]

45. Espósito BP, Najjar R. Coord Chem Rev 2002;232:137–149.

pyrophosphate   bisphosphonate   risedronate
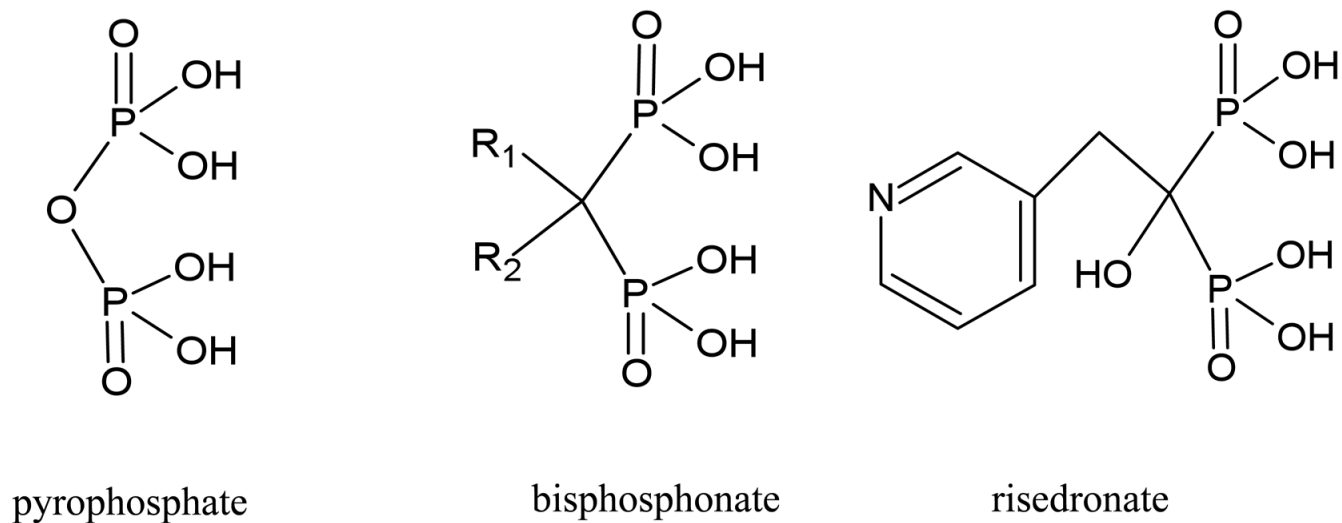
Figure 1.
General pyrophosphate, bisphosphonate and risedronate structures (acid forms).
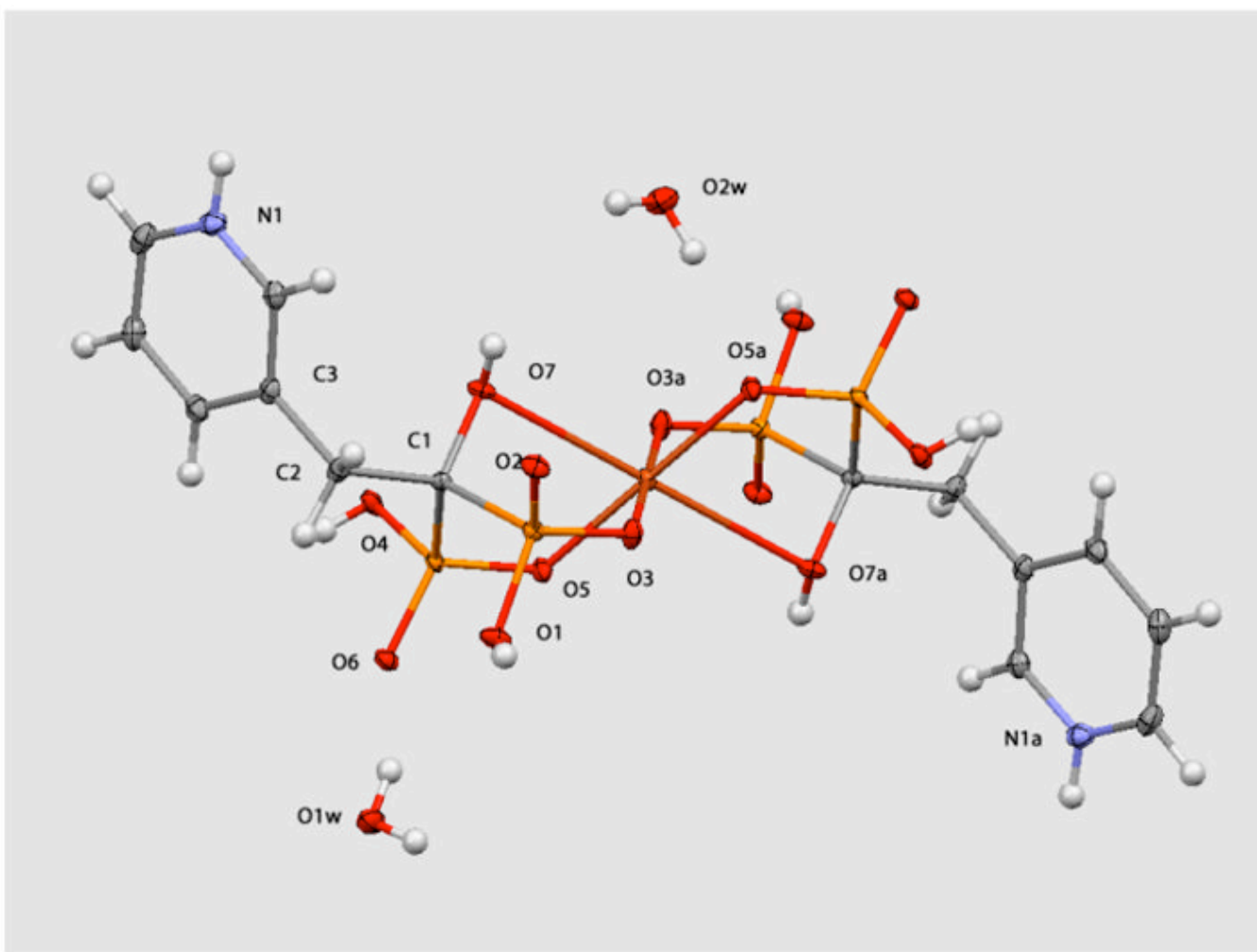
Figure 2.
Molecular structure of [Cu^{II}(Ris)$_2$]·4H$_2$O, showing ellipsoids at 50% probability level. The centrosymmetric water molecules O1wa and O2wa were omited for clarity.
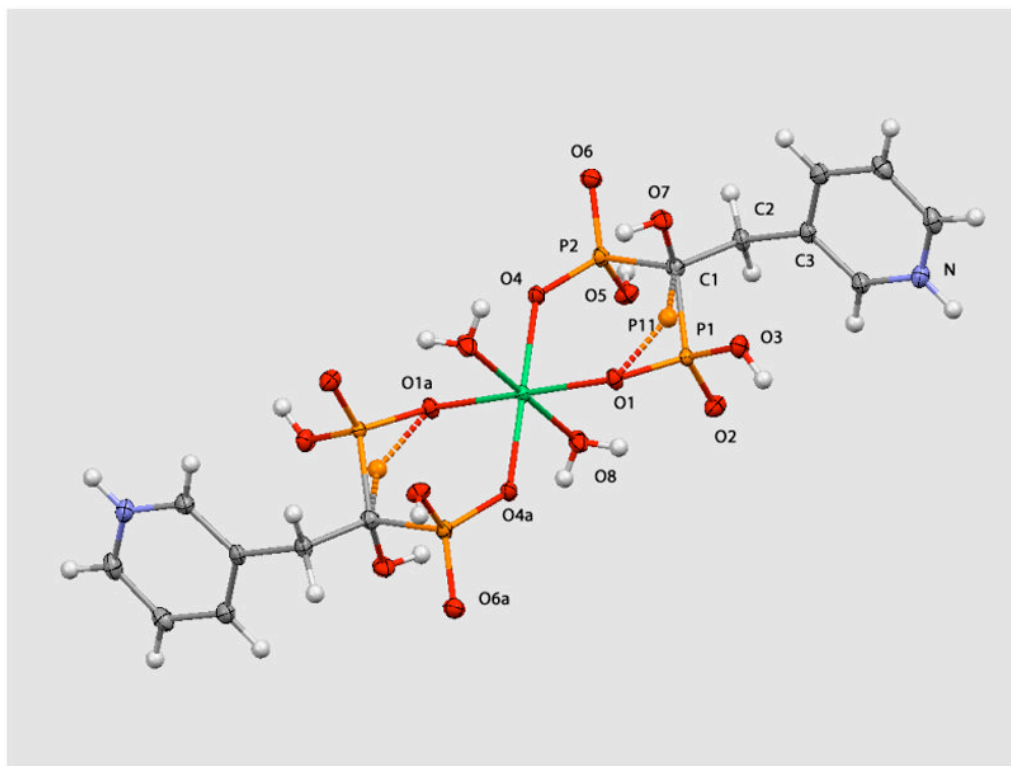
Figure 3.
Molecular structure of [Ni^{II}(Ris)$_2$(H$_2$O)$_2$] showing ellipsoids at 50% probability level. Atom P1 is disordered as shown by its equivalent labeled P11 in ball style, i.e. in most molecules the phosporus occupies the P1 position, in the others it is in the P11 site. Non coordinated water molecules are not shown for clarity.
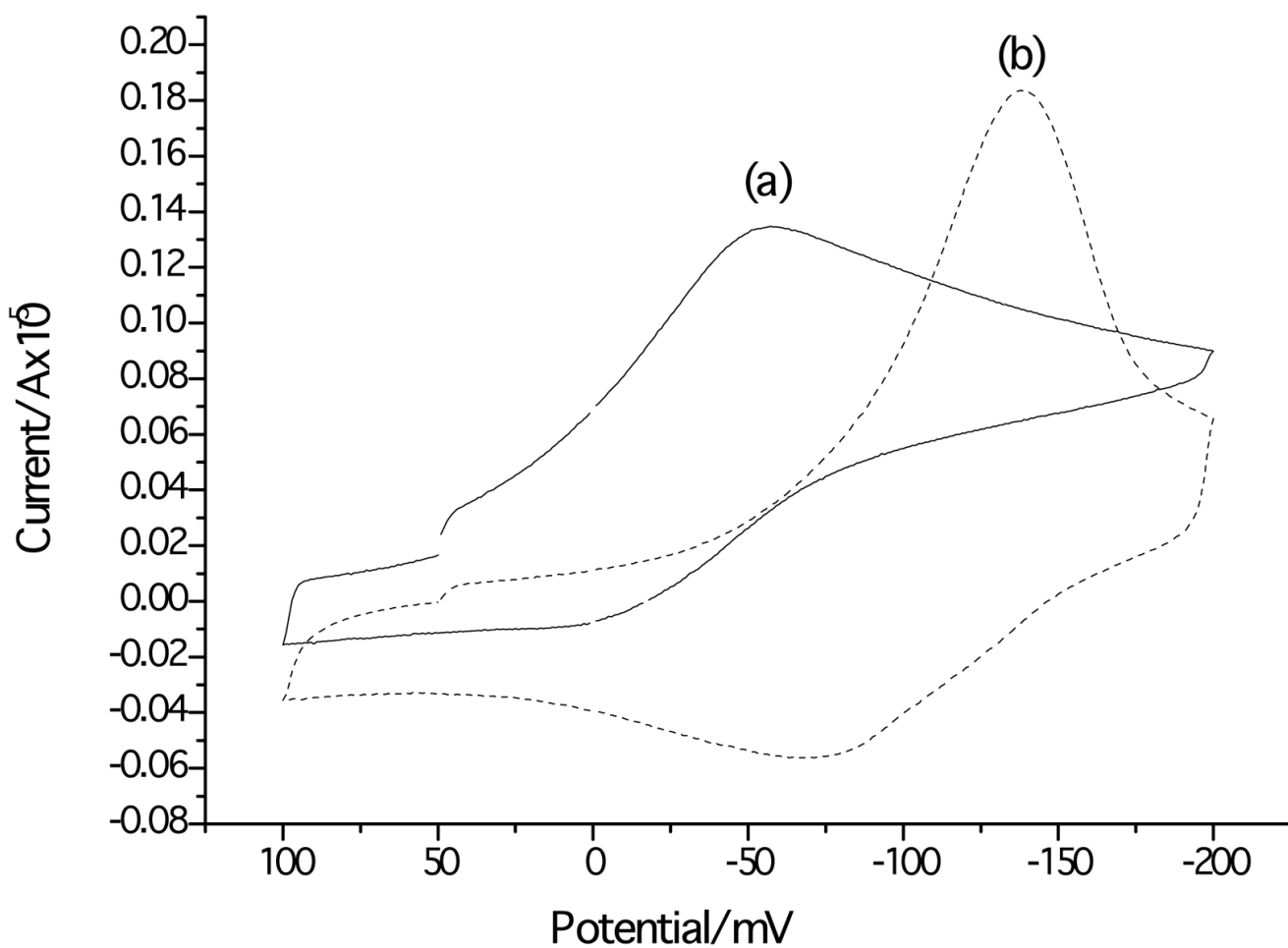
Figure 4.
Cyclic voltammograms of 0.5mM (a) $CuCl_2$ (b) $[Cu^{II}(Ris)_2]$ in aqueous solutions (phosphate buffer 0.1 M, pH=7) at scan rate v = 100 mV/s.

Table 1

X-ray data of $[Cu^{II}(Ris)_2]\cdot 4H_2O$ and $[Ni^{II}(Ris)_2(H_2O)_2]\cdot 2H_2O$

Empirical formula	$C_{14}H_{28}CuN_2O_{18}P_4$	$C_{14}H_{28}N_2NiO_{18}P_4$
Crystal color	sky blue	light green
Formula weight	699.81	694.95
Crystal System, Space group, habit	Triclinic, P-1, prismatic	
a (Å)	7.6505(4)	6.6792(3)
b (Å)	8.5866(5)	9.6383(4)
c (Å)	10.2793(6)	9.7242(5)
α(°)	65.952(1)	97.695(1)
β(°)	84.968(1)	93.744(1)
γ(°)	78.875(1)	99.829(1)
Volume (Å^3)	605.04(6)	608.77(5)
Z, density (mg/mm^3)	1, 1.921	1, 1.896
Absorption coefficient	1.260	1.152
Crystal size (mm)	$0.17 \times 0.11 \times 0.05$	$0.24 \times 0.20 \times 0.15$
θ range data collection	2.17, 28.27	1.152, 28.28
Limiting índices	−10, 10/−11, 11/−13, 13	−8, 8/−12, 12/−12, 12
Data collected/unique	8056/2990	8010/3001
Max, min. Transmission	0.81/0.94	0.77, 0.84
Refinement method	F^2	
Refined data/parameters	2740/210	2901/208
Goodness-of-fit on F^2	1.053	1.089
Final R, Rw [I>2sigma(I)]	0.0243, 0.0629	0.0265/0.0705
Weighing details	$w = 1/s^2(Fo^2)+(0.0306\ P)^2 + 0.4761P$, $P = (Fo^2 + 2Fc^2)/3$	$w = 1/s^2(Fo^2)+(0.0338\ P)^2 + 0.6134P$, $P = (Fo^2 + 2Fc^2)/3$

Table 2

Relevant intra-molecular bond distances and angles around the metal ion in $[Cu^{II}(Ris)_2]\cdot 4H_2O$ and $[Ni^{II}(Ris)_2(H_2O)_2]\cdot 2H_2O$

$[Cu^{II}(Ris)_2]\cdot 4H_2O$		$[Ni^{II}(Ris)_2(H_2O)_2]\cdot 2H_2O$	
distances (Å)			
Cu – O3	1.946(1)	Ni-O1	2.063(1)
Cu – O5	1.956(1)	Ni-O4	2.040(1)
Cu – O7	2.655(1)	Ni-O8	2.071(1)
angles (°)			
O5 – Cu – O3	89.74(5)	O1 – Ni – O4	90.82(4)
O5 – Cu – O3a	90.26(5)	O1 – Ni – O8	88.85(5)
O5 – Cu – O7	77.60(5)	O1 – Ni – 4a	89.18(4)
O5 – Cu – O7a	102.00(5)	O1 – Ni – O8a	91.15(5)
O3 – Cu – O7	78.20(5)	O4 – Ni – O8	88.31(5)
O3 – Cu – O7a	101.80(5)	O4 – Ni – O8a	91.69(5)
O3 – Cu – O3a	180	O1 – Ni – O1a	180
O5 – Cu – O5a	180	O4 – Ni – O4a	180
O7 – Cu – O7a	180	O8 – Ni – O8a	180

Table 3

Reduction peak potentials, in V, corresponding to 0.5 mM aqueous solutions (phosphate buffer 0.1 M, pH=7) at v = 100 mV/s scan rate, of metal risedronate complexes and the corresponding metal salts. Values measured in the conditions reported for the experiments.

Compound	E (V)	Compound	E (V)
$[Mn^{II}(Ris)_2]$	− 0.210	$[Ni^{II}(Ris)_2]$	− 0.091
$MnCl_2$	− 0.083	$NiCl_2$	− 0.077
$[Co^{II}(Ris)_2]$	− 0.163	$[Cu^{II}(Ris)_2]$	− 0.138
$CoCl_2$	− 0.080	$CuCl_2$	− 0.057

Table 4

In vitro anti *T. cruzi* activity of obtained Ris complexes

Compound	PGI$_{25\mu M}$ (%)[a] (epimastigote)	IC$_{50}$ (μM)[b] (amastigote)	IC$_{50}$ (μM)[c] (FPPS)
NaRis	19	55 ± 5	0.0270 ± 0.009
[Cu^{II}(Ris)$_2$]	16	23 ± 7	0.0260±0.0048
[Ni^{II}(Ris)$_2$]	23	34 ± 10	0.0029±0.0012
[Co^{II}(Ris)$_2$]	32	> 50	> 0.1
[Mn^{II}(Ris)$_2$]	35	14 ± 4	0.0027±0.0014

[a]PGI: percentage of growth inhibition of *T. cruzi* epimastigote cells at 25 μM concentration of the complexes.

[b]Concentration of complexes inhibiting 50 % growth of *T. cruzi* amastigotes.

[c]Concentration of complexes inhibiting 50 % activity of TcFPPS.

Table 5

Level of BSA binding of the obtained complexes after 48 h incubation

Compound	Complex bound to BSA (%)
[Mn^{II}(Ris)$_2$]	67
[Co^{II}(Ris)$_2$]	87
[Cu^{II}(Ris)$_2$]	64
[Ni^{II}(Ris)$_2$]	91